EBioMedicine 64 (2021) 103236

Contents lists available at ScienceDirect

EBioMedicine

journal homepage: www.elsevier.com/locate/ebiom

Research paper

Simpler and faster Covid-19 testing: Strategies to streamline SARS-CoV-2 molecular assays

Nuttada Panpradist[a,b], Qin Wang[a], Parker S. Ruth[a,c], Jack H. Kotnik[a,d], Amy K. Oreskovic[a], Abraham Miller[a], Samuel W.A. Stewart[a,e], Justin Vrana[a], Peter D. Han[g,h], Ingrid A. Beck[e], Lea M. Starita[g,h], Lisa M. Frenkel[e,f,*], Barry R. Lutz[a,h,*]

[a] Department of Bioengineering, University of Washington, Seattle, WA, United States
[b] Global Health of Women, Adolescents, and Children (Global WACh), School of Public Health, University of Washington, Seattle, WA, United States
[c] Paul G. Allen School of Computer Science & Engineering, University of Washington, Seattle, WA, United States
[d] Department of Family Medicine, University of Washington, Seattle, WA, United States
[e] Center for Global Infectious Disease Research, Seattle Children's Research Institute, Seattle, WA, United States
[f] Departments of Global Health, Medicine, Paediatrics, and Laboratory Medicine, University of Washington, Seattle, WA, United States
[g] Department of Genome Sciences, Seattle, WA, United States
[h] Brotman Baty Institute for Precision Medicine, Seattle, WA, United States

ARTICLE INFO

Article History:
Received 6 July 2020
Revised 15 January 2021
Accepted 22 January 2021
Available online xxx

Keywords:
Low-cost Covid-19 testing
Fast Covid-19 testing
Point-of-care

ABSTRACT

Background: Detection of SARS-CoV-2 infections is important for treatment, isolation of infected and exposed individuals, and contact tracing. RT-qPCR is the "gold-standard" method to sensitively detect SARS-CoV-2 RNA, but most laboratory-developed RT-qPCR assays involve complex steps. Here, we aimed to simplify RT-qPCR assays by streamlining reaction setup, eliminating RNA extraction, and proposing reduced-cost detection workflows that avoid the need for expensive qPCR instruments.
Method: A low-cost RT-PCR based "kit" was developed for faster turnaround than the CDC developed protocol. We demonstrated three detection workflows: two that can be deployed in laboratories conducting assays of variable complexity, and one that could be simple enough for point-of-care. Analytical sensitivity was assessed using SARS-CoV-2 RNA spiked in simulated nasal matrix. Clinical performance was evaluated using contrived human nasal matrix ($n = 41$) and clinical nasal specimens collected from individuals with respiratory symptoms ($n = 110$).
Finding: The analytical sensitivity of the lyophilised RT-PCR was 10 copies/reaction using purified SARS-CoV-2 RNA, and 20 copies/reaction when using direct lysate in simulated nasal matrix. Evaluation of assay performance on contrived human matrix showed 96.7–100% specificity and 100% sensitivity at ≥20 RNA copies. A head-to-head comparison with the standard CDC protocol on clinical specimens showed 83.8–94.6% sensitivity and 96.8–100% specificity. We found 3.6% indeterminate samples (undetected human control), lower than 8.1% with the standard protocol.
Interpretation: This preliminary work should support laboratories or commercial entities to develop and expand access to Covid-19 testing. Software guidance development for this assay is ongoing to enable implementation in other settings.
Fund: USA NIH R01AI140845 and Seattle Children's Research Institute

1. Introduction

Severe acute respiratory syndrome coronavirus 2 (**SARS-CoV-2**), the causative viral pathogen to coronavirus disease 2019 (**Covid-19**), has infected millions of people in more than 180 countries worldwide. Estimates suggest that 1.3% of diagnosed infections are fatal [4], and there is mounting evidence that many infected people have mild or no symptoms but can unknowingly spread the disease [5,6]. To contain the Covid-19 pandemic, many countries have adopted 'lockdown' measures, which drastically impact the global economy [7]. Rapid and low-cost SARS-CoV-2 tests can sustainably enable diagnosis, contact tracing and isolation of exposed individuals at a global scale, making these tests essential for lifting confinement restrictions and re-opening the global economy whilst continuing to

* Corresponding authors.
E-mail addresses: lfrenkel@uw.edu (L.M. Frenkel), blutz@uw.edu (B.R. Lutz).

https://doi.org/10.1016/j.ebiom.2021.103236

Research in context

Evidence before this study

Currently the World Health Organization and US Centers for Disease Control and Prevention (**CDC**) recommend use of molecular tests to detect acute infection of severe acute respiratory syndrome coronavirus 2 (**SARS-CoV-2**), the pathogen that causes coronavirus disease 2019 (**Covid-19**). We have conducted an in-depth analysis of commercially available RT-PCR tests for **SARS-CoV-2** detection up to April 23rd, 2020. Out of 41 molecular tests that received the US FDA Emergency Use Authorization, 37 are RT-PCR based assays. Due to their complexity, most RT-PCR assays are only approved for operations in Clinical Laboratory Improvement Amendments (**CLIA**)-certified laboratories. A new point-of-care test, Abbott IDNow®, relies on novel reverse transcription recombinase polymerase amplification (**RT-RPA**) chemistry and can provide positive results as fast as 13 min (1 patient specimen/machine run) [1]. Although RT-RPA is fast, high false negative rates were observed in several studies [2, 3].

Added value of this study

Instead of looking towards new amplification chemistry, we developed and adapted techniques, hardware, and software to simplify existing RT-PCR assays. The result is an easy-to-use platform which enables assay operators to set up an RT-PCR assay in minutes, with results available after 90 min. Keeping in mind that most resource-limited settings do not have access to expensive real-time thermal cyclers or consistent electrical power, we also developed an RT-PCR workflow that requires only battery-powered, low-cost instruments and reagents. A newly developed software algorithm can accurately classify positive and negative tube images taken by different cell phone models, including some commonly used in Asia and Africa.

Implications of all the available evidence

We present RT-PCR assay workflows that are simpler, faster and lower-cost compared to the CDC assay, and successfully amplify SARS-CoV-2 RNA directly from human nasal swab eluates. The simplest workflow we present may allow SARS-CoV-2 RT-PCR testing at point-of-care settings. This test could become an important clinical tool for Covid-19 diagnosis and management in a time when the world desperately needs fast, reliable, low-cost, and rapidly deployable SARS-CoV-2 diagnostic capabilities.

limit transmission [8]. Several FDA-approved antibody rapid tests for SARS-CoV-2 are relatively economical but serve primarily to detect past infection, and have variable sensitivity and specificity [9]. Several antigen detection tests were approved for diagnosis of acute SARS-CoV-2 infection, but they are less sensitive compared to nucleic acid amplification tests (**NAATs**) [2,10]. Presently, the World Health Organization (**WHO**) and US CDC recommends NAATs for diagnosis of acute infection. Numerous commercially-available NAATs received emergency use authorization (**EUA**) through the U.S. Food and Drug Administration (**US FDA**), the European CE Marking for In Vitro Diagnostic (**IVD**) devices, or WHO pre-qualification [11]. All require non-traditional, expensive equipment and reagents.

In this work, we developed and applied engineering approaches to simplify existing molecular methods applied to the SARS-CoV-2 EUA assay from the **CDC** as our model assay [12,13] . The US CDC RT-qPCR assay detects SARS-CoV-2 nucleoprotein transcripts using two primer sets (**N1** and **N2**) and human Rnase P transcripts (**RP**) as an extraction/amplification control. Amplification of these RNA transcripts is tracked in separate reactions via hydrolysis of FAM/ZEN™ probes that occur as *Taq* polymerase amplifies the targets. The changes in fluorescence contributed from the target amplification are typically tracked at the end of each temperature cycle by a real-time thermal cycler. To expand access to real-time RT-qPCR assay, we developed strategies to simplify assay workflows. Previously, our group developed and validated a software-guided workflow for nucleic acid genotyping tests to detect HIV drug resistance and showed that this workflow could be successfully performed by first-time non-trained users [14,15]. Here, we applied similar strategies to improve access to SARS-CoV-2 RT-PCR based testing. First, we developed and optimised a lyophilised RT-PCR formulation, achieving analytical sensitivity comparable to that of the standard US CDC EUA protocol [16]. Second, we eliminated the need for nucleic acid extraction from nasal swab specimens, adding swab eluate/lysate directly to RT-PCR reaction. Third, we designed three different workflow scenarios based on access to equipment, including the use of a new software to analyse end-point fluorescence tube images obtained by various cell phone models. Last, we validated the assay performance using contrived human nasal specimens (SARS-CoV-2 RNA spiked in human nasal matrix) and clinical nasal specimens. Together, this work will help simplify RT-PCR assays across both high-resource labs and point-of-care settings by reducing turnaround time, cost, and equipment needs.

2. Methods

2.1. Preparation of analytical specimen panel

In this study, we used mid-turbinate nylon swabs (Copan Diagnostics Inc., 56380CS01). Each swab was loaded with 15 μL of simulated nasal matrix (1% *(w/v)* mucin porcine stomach type III, 10 mg/mL human genomic DNA, and 110 mM sodium chloride) [17] and dried for 30 min. Swabs were resuspended in 1x lysis/rehydration buffer containing 2 mM MgSO4, 0.5% *(v/v)* Triton X-100, and 1x buffer (New England Biolab B9023SVIAL). 18 μL or a droplet from a dropper of swab elution was used to rehydrate a lyophilised RT-PCR reaction using micropipettes (Ranin XLS L8−20) or dropper (Nalgene 69047). Rehydrated RT-PCR reactions without or with SARS-CoV-2 RNA at different concentrations were subjected to RT-PCR.

2.2. Preparation of clinical specimen panel

Human nasal swabs (n = *41*) were collected on Puritan™ Polyester-Tipped Applicators (Fisher) by health care workers and tested in the Frenkel CLIA-certified laboratory at Seattle Children's Research Institute. The swabs were resuspended in 1 mL 1xPBS and stored at 4 °C until testing. These swabs were tested for SARS-CoV-2 and shown to be negative. Additionally, we obtained remnant human respiratory specimens that were collected from individuals (n = 110) presenting respiratory symptoms, by observed or unobserved collection using mid-turbinate swabs (Copan) or nasopharyngeal swabs collected by healthcare workers. Swabs were stored in 3 mL viral transport medium (Becton Dickinson 220220), aliquoted, and stored at −80 °C until testing.

2.3. Preparation of in-vitro SARS-CoV-2 RNA transcript

Synthetic SARS-CoV-2 gBlock (Integrated DNA Technology) containing the consensus sequence (NCBI up to January 2020) was used as the template to generate RNA via in-vitro RNA transcription by Hi-T7 RNA polymerase (New England Biolabs, M0658S), following the protocol from the manufacturer. The RNA was quantified using Qubit RNA HS Assay Kit (Invitrogen, Q32852). Fragment size and integrity

of the in-house RNA was confirmed using Tapestation High Sensitivity RNA ScreenTape (Agilent 5067-5579). The in-house RNA showed expected size with no sign of degradation and its concentration was quantified using digital droplet PCR (Stilla, Naica® system workflow) according to the manufacturer's protocol.

2.4. Preparation of lyophilised RT-PCR reagents

10 μL of magnesium-free RT-PCR mixture contained 2x primer/probe (IDT 10-006-770, sequences are accessible from CDC website [12]), 10 mM DTT, 16.881.6% *(w/v)* trehalose, 400 μM ea. dNTPs, 2 units of OneTaq® Hot-start polymerase (NEB M0481X), 6 units of RTx WarmStart™ (NEB M0380L), and 0.025x RNasIn Plus (NEB N2115). The mixture was submerged into liquid nitrogen for 2 min and dried at 0.018 mbar, −55 °C. Lyophilised reagents were stored with desiccant packets in sealed foil pouches until use.

2.5. Setting up RT-PCR reactions

RT-PCR reactions were rehydrated in 1x lysis/rehydration buffer in water for purified RNA experiment in Section 3.1 and swab eluates in the rest of the experiments. The rehydrated RT-PCR reaction either without (no template control) or with SARS-CoV-2 RNA was then subjected to a cycle run either in a real-time thermal cycler (CFX96 Touch, BioRad), standard thermal cycler (T100, BioRad), and a battery-powered thermal cycler (Mini-16, MiniPCR) of 8 min at 55 °C, 2 min at 94 °C and 50 cycles of 1 second 94 °C and 30 s at 57 °C. In the RT-qPCR experiment, the plate read step via FAM dye channel was performed at the end of each extension cycle. For nasal swabs eluted in 1xPBS, either 1:2, 1:4, or undiluted swab eluates mixed with the lysis buffer were added to lyophilised RT-PCR reagents with or without SARS-CoV-2 RNA at different concentrations before undergoing RT-PCR. For nasal viral transport medium (**VTM**) samples, 1:4 diluted swab eluate was added to lyophilised RT-PCR before undergoing RT-PCR. For the standard protocol, 5 μL of extracted RNA was added to 15 μL RT-PCR mix according to the CDC guideline [13].

2.6. Analysis of RT-QPCR results

The CFX96 Touch instrument (BioRad) was used to operate RT-qPCR runs. Biorad CFX Maestro software was used to determine the quantification cycle (Cq) of the samples.

2.7. Analysis of images from transilluminator and glow box

Images of reaction tubes after completion of the RT-PCR were obtained using a transilluminator or a glow-box and the default Android cell phone camera application without any assisted applications. The fluid-filled tips of the vials were segmented by applying a manually set threshold to the norm of the distance in Red-Green-Blue (**RGB**) space; the distance metric was computed relative to the average RGB pixel value of a positive control sample. Binary opening and closing was applied to the thresholded image to fill holes and remove noise. The tube regions were then selected with a heuristic algorithm. After segmenting tube regions, the mean RGB value for each tube was computed inside the region of interest. For the glow box images, the specular reflections were eliminated by performing k-means clustering on the region of interest pixel values. The mean RGB pixel values for each scenario and phone model were converted to intensity values using a support vector machine (**SVM**) with a linear kernel. P-values and confidence intervals were numerically computed as described in Section 2.11.

2.8. Analytical sensitivity assessment

Single-used purified RNA transcript aliquots were stored at −80 °C at a concentration of 2×10^8 copies/μL and diluted fresh for each experiment to 2.5, 3.5, 5, 10, 100, 10^3, 10^4, and 10^5 copies/μL. 2 μL of RNA sample or water (for no template control) were added to 18 μL RT-PCR mix to achieve the final volume of 20 μL.

2.9. Validation testing in clinical specimens

To test assay accuracy in human nasal matrices, 41 nasal swab eluates (collected in May 2020 from non-symptomatic individuals and tested negative for SARS-CoV-2 RNA) were used to generate contrived specimens for accuracy testing: 41 negative, 21 positive at 100 copies RNA/reaction, 10 positive at 40 copies RNA/reaction, and 10 positive at 20 copies RNA/reaction (1x LoD). For the Scenario 3 workflow, we tested 30 negative, 6 positive at 100 copies RNA/reaction, 16 positive at 40 copies RNA/reaction, and 8 positive at 20 copies RNA/reaction. In addition to contrived nasal specimens, we analysed remnant upper respiratory specimens, collected from November 2019 – April 2020. These specimens were positive (n = 40) and negative (n = 70) for SARS-CoV-2 RNA, as determined by the protocol previously described [18]. Presence of adenovirus, seasonal coronavirus, influenza, respiratory syncytial virus, parainfluenza virus, metapneumovirus, enterovirus, parechovirus, bocavirus, and pneumoniae were also tested in these specimens using TaqMan® OpenArray™ Respiratory Tract Microbiota Plate (Thermo Fisher A41237). We performed both standard and modified protocols on these specimens. For the standard protocol, 100 μL each sample was extracted (Qiagen 52-906) following the CDC protocol, except the purified RNA was eluted in 70 μL (instead of 100 μL). 5 μL purified RNA was subsequently added to 15 μL RT-PCR mixture according to the standard CDC protocol. For the modified workflow, 5 μL each sample was directly added to each 15 μL rehydrated, lyophilised RT-PCR. Cq values of the paired samples were compared. Discordant results from the standard and modified protocols were verified using previous analysis by the University of Washington Virology lab. Additionally, end-point fluorescence of each N1, N2, and RP assays was plotted to determine its feasibility to classify positive from negative samples.

2.10. Ethics

All specimens were left-over from previous studies at the Frenkel lab at Seattle Children's Research Institute and the Starita lab at the University of Washington. Nasal swabs were collected and tested for SARS-CoV-2 infection as part of the Seattle Children's SARS2 Prospective Cohort, as approved by the Seattle Children's Institutional Review Board (IRB#: STUDY00002434) and as part of the Seattle Flu Study, as approved by the Institutional Review Board at the University of Washington (IRB#: STUDY0006181). Informed consent was obtained for all participant samples, including for use of de-identified, remnant specimens.

2.11. Statistical analysis

Number of specimens tested in each experiment are reported in the method section or at the specific figure legends. To assess the accuracy of our tests, we performed a power calculation using binomial cumulative distribution function. A minimum sample size of 30 was required to achieve the confidence interval (**CI**) of 90−100% should all results be accurate. We selected a sample size, n, such that a 95% confidence interval for p included 0.9−1 which, based on our previous work, was likely to be the proportion of accurate tests. The upper bound of this confidence interval was 1. The lower bound was the largest value of p for which the $P(X < 0.05)$, where X~binomial (n, 0.9). Mean, CI, and standard deviations (**SD**) were provided along

with individual data points in each experiment. To evaluate the statistical significance of the SVM classifier outputs, we developed a nonparametric numerical p-value. For each dataset, we randomly shuffled the positive and negative class labels 1000 times, retraining the SVM and computing ROC AUC values for each; the p-value was the number of AUC values greater than or equal to the observed AUC value. We chose this method because it avoids assumptions of large dataset size or normality. To quantify the uncertainty of the AUC values for dataset, we computed confidence intervals using a parametric numeric simulation. For each dataset, we added gaussian noise to the RGB pixel values extracted from the tubes. The covariance of the gaussian noise was estimated from the covariance of the observed RGB data. To account for the effect of different copy numbers on the tube color variance, the noise covariance was estimated after subtracting the means from each set of tube replicates. An SVM was retrained for 10,000 independent gaussian noise additions, and the resulting distribution of AUC values gave bounds for the confidence intervals.

2.12. Role of funder

Research reported in this publication was supported by the National Institute of Allergy and Infectious Diseases of the National Institutes of Health under award number R01AI145486−01A1 and Seattle Children's Institute. The content is solely the responsibility of the authors and does not necessarily represent the official views of the National Institutes of Health or Seattle Children's Research Institute. The funders had no roles in study design, result interpretation in this study, or writing this report.

3. Results

3.1. Development of lyophilised RT-PCR reagents for SARS-CoV-2 RNA detection and analytical sensitivity of our protocol compared to the CDC protocol

Instead of using RT-PCR mix listed on the US CDC protocol [13], we chose to develop a new RT-PCR formulation that *(i)* is compatible with detergent-based lysis buffer and other contaminants from simulated nasal matrix containing mucin, human genomic DNA, and salts; *(ii)* contains cryoprotectant to stabilize RT-PCR reactions during lyophilization and *(iii)* maintains sensitivity comparable to the CDC RT-PCR assay. The assay uses the same primers and probes as the CDC protocol, but for the master mix we chose the combination of the warm-start reverse transcriptase, RTx WarmStart®, and the hot-start OneTaq® DNA polymerase. We found that the two enzymes are compatible, and both are resistant to mild detergents present in the lysis buffer (**Supplementary Fig. 1**). Trehalose, a universal cryoprotectant and protein thermal stabiliser [19], was used for lyophilization. We optimised the annealing/extension temperature in the presence of different trehalose concentrations to achieve the highest analytical sensitivity (**Supplementary Fig. 2**). We selected 8.4% w/v trehalose coupled with 57 °C annealing temperature for the base assay.

Analytical sensitivity (i.e. Limit of Detection (**LoD**)) of lyophilised RT-PCR with human genomic DNA background is 10 and 5 SARS-CoV-2 RNA copies/reaction for N1 (**Fig. 1A**) and N2 (**Fig. 1B**) assay, respectively. In some cases, we were able to detect 7 copies/reaction for N1. **Fig. 1C** shows an overview comparison of our modified protocol and the CDC protocol. In the CDC protocol, 5 μL RNA sample was added to 20 μL RT-PCR reaction. In contrast, our lyophilised reaction can be entirely rehydrated with 20 μL RNA sample. Thus, the analytical sensitivity of 10 copies/reaction is equivalent to a 0.5 ($10^{-0.3}$) RNA copies/μL sample. For direct comparison, we analysed spiked-in SARS-CoV-2 RNA in viral transport medium according to the CDC protocol. We observed the analytical sensitivity of 5 copies/reaction, equivalent to 1 (10°) RNA copy/μL sample, matching the reported analytical sensitivity by CDC (**Fig. 1D**).

Next, we demonstrated direct amplification of swab eluate without an RNA extraction step. The swab elution buffer used in our workflow is multipurpose. It is used to directly rehydrate the lyophilised reagents to run the assay. The detergent present in the buffer will also lyse the virus in conjunction with the mild heating at the 55 °C reverse transcription step. We tested the lysing efficiency by using our lyophilised N2 assay to directly amplify the intact AccuPlex™ virus control – a SARS-CoV-2 RNA control that is packaged within a viral protein envelope. Our RT-PCR assay detected 25 copies of the control virus, and the mixture of enveloped RNA and swab elution buffer stored for 2 h at 4 °C had similar results to the fresh lysate (**Supplementary Fig.3**). We also assessed the effects of potential inhibitors that may be present in human nasal samples. We first used human DNA spiked in porcine simulated nasal matrices and salts, similar to formulations used to evaluate US FDA-cleared influenza tests (e.g. Xpert® Flu [20]). We amplified SARS-CoV-2 naked RNA in the presence of the simulated nasal matrix and lysis buffer showing analytical sensitivity of 20 copies/reaction, equivalent to 1 (10^0) RNA copy/μL (**Fig. 1D**).

For comparison, we compiled the reported sensitivities on existing EUA authorised approved molecular assays (up to April 23rd, 2020) and created a frequency distribution plots of the LoD based on the copy number of purified RNA (**Fig. 1D,** purified RNA copy/μL eluates after extraction) and the copy number in original swabs prior to extraction (**Fig. 1E**, RNA copies/swab sample). The LoD of our lyophilised RT-qPCR is in the middle range of the LoD from the available tests and lower than or comparable to that of the CDC assay.

3.2. Scenario 1 – high-throughput RT-qPCR workflow for laboratories

Fig. 2A shows a diagnostic testing workflow designed for a high-throughput lab that first screens for infection using a more sensitive SARS-CoV-2 assay (i.e. N2 primer set) and the human control (i.e. RP primer set). Only samples positive for N2 would then be confirmed with primers for N1. This Scenario 1 workflow requires a single-channel real-time thermal cycler (see example models and listed prices in **Supplementary Table 2**), and optional multichannel micropipettes to allow faster parallel processing of samples. The streamlined workflow (**Fig. 2B**) begins with the elution of dry swabs in barcoded racked tubes containing 300 μL elution/rehydration buffer. Each barcode would be associated with both a patient ID and its designated location on the 96-well rack. We chose 300 μL because it is the lowest volume that can provide sufficient dilutions of inhibitors from the sample as well as enough volume to run three RT-PCR reactions. 20 μL eluate from each swab is directly transferred to the lyophilised RT-PCR plate. The plate with the rehydrated RT-PCR mixtures is then sealed and run in a real-time thermal cycler using the RT-PCR protocol. The analytical sensitivity of this assay using SARS-CoV-2 RNA in background eluate from simulated nasal matrix is 20 copies/reaction, corresponding to a starting RNA concentration of 1 (10^0) copy/μL eluate (**Fig. 2C**) and 300 ($10^{2.48}$) copies/swab sample (**Fig. 2D**).

3.3. Scenario 2 – high throughput laboratory end-point RT-PCR workflow

For laboratories without access to a real time thermal cycler, we propose the Scenario 2 workflow where a standard 96-well thermal cycler (**Supplementary Table 3**) and a low-cost fluorescence reader can be employed (**Supplementary Table 4**), together with a phone-based image processing software. Similar to Scenario 1, the lyophilised RT-PCR can be rehydrated directly by swab eluates and tested using the same diagnostic algorithm presented in **Fig. 2A**. However, in this Scenario 2 workflow (**Fig. 3A**), laboratories can reduce the cost of required equipment whilst maintaining high assay throughput. As

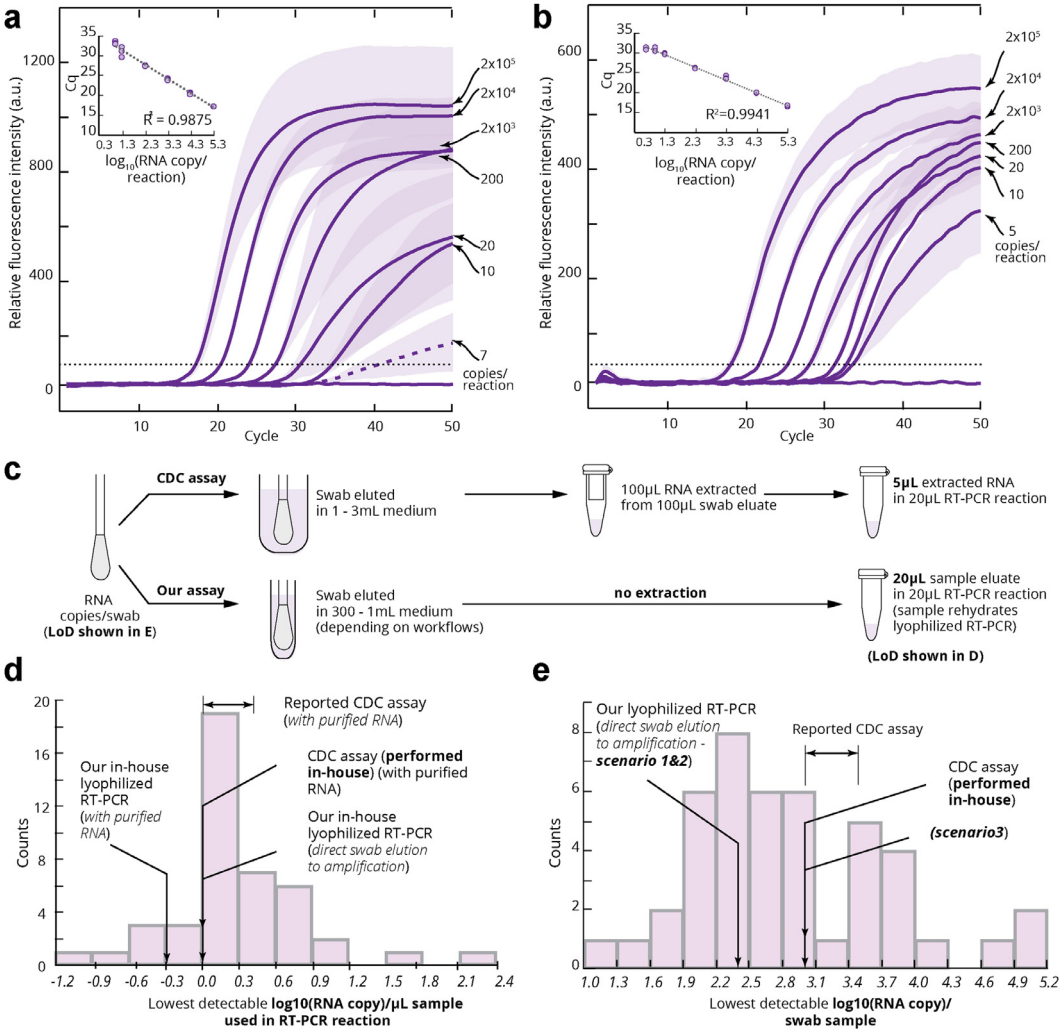

Fig. 1. *Analytical sensitivity of a newly-developed lyophilised RT-qPCR formulation using CDC primers/probes.* (**A**) N1 and (**B**) N2 assay amplification curves of SARS-CoV-2 RNA at 0, 5 or 7, 10, 20, 200, 2×10^3, or 2×10^4 copies in the presence of 1 ng human genomic DNA (3 technical replicates, mean ± SD). Dashed amplification curve shows average of the 2/3 replicates of 7 copies/reaction for N1 assay. Dotted horizontal lines in (A) and (B) indicate the detection threshold that defines the quantification cycle (Cq). The insets of each plot show RT-PCR efficiency plot. (**C**) Workflow comparison between the CDC protocol and our assay (**D**) Histogram of the reported LoD ($\log_{10}$P of RNA copy/**μL eluate**) from the existing EUA molecular assays, CDC protocol performed in-house, and our lyophilised RT-PCR assay. Note that extraction efficiencies were not reported, and 100% extraction efficiency was assumed to calculate the $\log_{10}$ (RNA copy/μL eluate). CDC assay reported two LoDs from the two recommended RNA extraction kits, so we indicated the range of LoD in the histogram (i.e. $10^0 - 10^{0.4}$ copies/μL) of the CDC assay. (**E**) Histogram of the reported LoD ($\log_{10}$ of RNA copy/**swab**) in existing EUA approved molecular assays, CDC protocol performed in-house, and our lyophilised RT-qPCR assay. Note that in the CDC protocol, swabs were eluted in at least 1 mL medium while our protocols used 300 μL - 1 mL depending on the scenario, which will be discussed (Sections 3.2–3.4). For (C) and (D), only tests that provided sufficient information in their EUA IFU to calculate the necessary values were included. Additionally, for tests that reported multiple analytical sensitivities depending on extraction methods, both were included. Refer to **Supplementary Table 1** for a complete summary.

in Scenario 1, during the annealing/extension step in RT-PCR, the polymerase enzyme hydrolyses the 5′ TaqMan™ probe and releases FAM signal proportionally to the amplified targets. The product of the RT-PCR step is temperature stable, and this end-point product can be read at ambient temperature under a transilluminator (**Fig. 3B**) or a battery-powered glow box (**Fig. 3C**). To the unaided eye, the no template control signals from the glow box image were not distinguishable from 20 copies/reaction. However, with software image processing (see details in Section 3.5), the analytical sensitivity of this assay is the same as the Scenario 1 workflow (20 copies/reaction) regardless of visualization tools used. Classification of negative and positive SARS-CoV-2 samples using software-analysed relative fluorescence intensities was excellent. Receiver operating characteristic area under the curve (**ROC AUC**) computed from the relative fluorescence intensities is 0.999 and 1, respectively, for transilluminator and glow box.

3.4. Scenario 3 – low throughput clinics with access to a battery-powered thermal cycler and fluorescence reader

In this scenario (**Fig. 4A**), users do not need access to micropipettes. Instead, a dropper container is used to dispense the lysate. The dry swab is resuspended in the bottle containing 1 mL of lysis/rehydration buffer. 1 mL of buffer is used in this scenario instead of 300 μL because the dropper has some dead volume. The dropper tip is then loaded onto the top of the bottle and used to dispense 20 μL of the lysate into each lyophilised RT-PCR reaction (N1 or N2 primer set to target SARS-CoV-2; and RP human control primer set). We chose a battery-powered thermal cycler to eliminate interruptions due to power outage, a common issue in low-resource settings. The analytical sensitivity of this assay is the same as the Scenario 1 workflow (20 copies/reaction) regardless of visualization tools used (**Fig. 4, B and C**). Differentiation of negative from positive SARS-CoV-

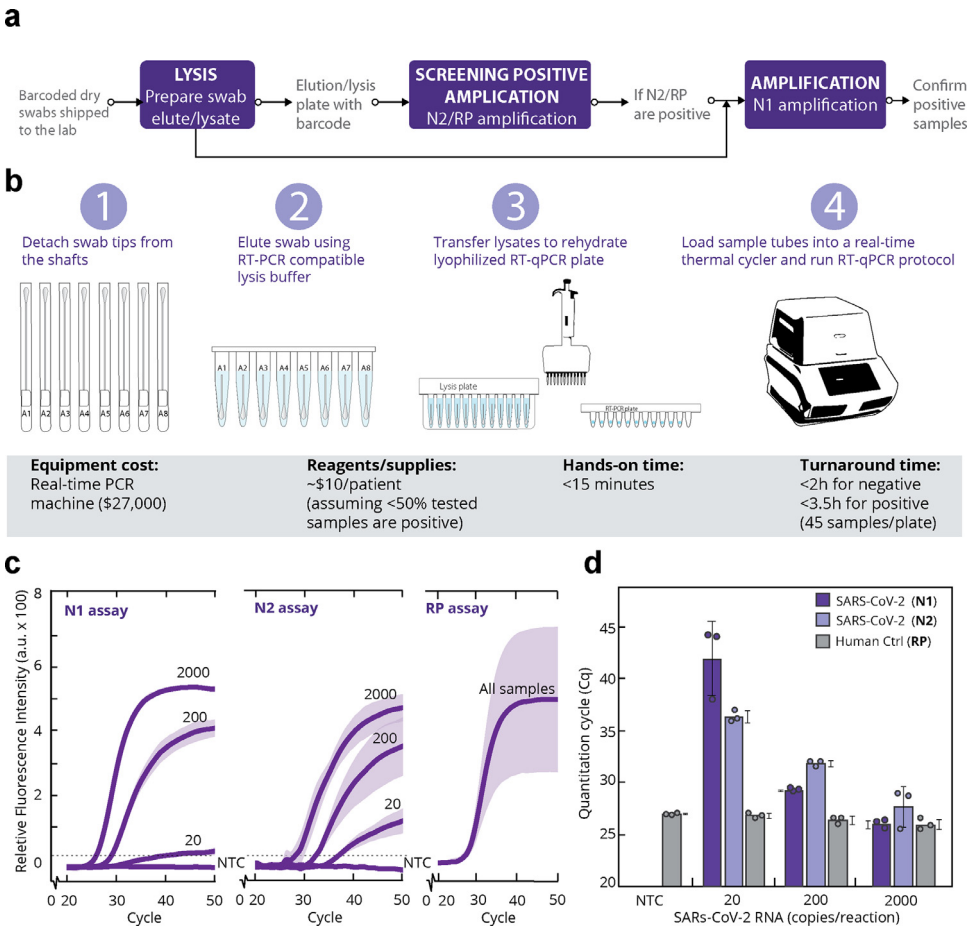

Fig. 2. *High-throughput laboratories with access to a real-time thermal cycler* **(A)** Diagnostic algorithm modified from the original CDC protocol to increase speed and cost-effectiveness. (**B**) Demonstration of high-throughput RT-qPCR workflow. Swab eluates are lysed and used directly in RT-qPCR. (**C**) Amplification curves of lyophilised RT-qPCR using N1, N2, and RP primers. 15 μL of simulated nasal matrix (1% w/v mucin, 110 mM NaCl, and 10 ng/μL human genomic DNA) were spiked on swabs and eluted in 300 μL lysis buffer (0.5% Triton-X 100, 2 mM $MgSO_4$ in water). 18 μL of lysate with 2 μL of SARS-CoV-2 RNA at 0 (no template control), 20, 200, 2000 copies/reaction were then subjected to RT-PCR. Relative fluorescence signal of each samples (3 technical replicates, mean ± SD) at the end of each amplification cycle were plotted. (**D**) Quantification cycles (Cq) of the samples tested using lyophilised RT-qPCR reactions with N1, N2 primers (SARS-CoV-2) or RP primers (positive human control) with 3 technical replicates, mean ± SD. Water control (no simulated nasal matrix) did not generate signals detectable by N2 primers. Equipment costs listed are based on the models we used in this study.

2 samples using software-analysed relative fluorescence intensities remained excellent. ROC AUC computed from the relative fluorescence intensities was 1 and 0.967, respectively, for transilluminator and glow box.

3.5. Software analysis of fluorescence tube images

All images in the previous experiments in the Scenario 2 and Scenario 3 workflows were captured using a single cell phone (i.e. OnePlus 7 Pro) to maintain consistency across experiments. The fluorescence of each image (**Supplementary Fig.4**) was quantified using a newly-developed image processing Python algorithm (**Fig. 5A**). We observed strong linear correlation of the end-point fluorescence signal measured by the real-time qPCR machine and the processed relative fluorescence signal from both the transilluminator (**Fig. 5B,** R^2=0.77, 95% CI: 0.67−0.87 Olkin and Kinn's approximation) and the glow box (**Fig. 5C,** R^2=0.84, 95% CI: 0.76−0.91). Additionally, we performed two-fold cross validation of the algorithm across four independent datasets, and observed excellent classification performance (**Supplementary Fig.5**) with the ROC AUC of 0.978 − 1.0 (mean ± SD: 0.991±0.009). Next, we investigated whether this software would be robust across images taken by different models of cell phones, including models used in the US and models commonly used in Asia and Africa (**Supplementary Table 5**). We observed dramatic differences in the quality of images taken by the cell phones, but software-processed images successfully distinguished between the no SARS-CoV-2 RNA template plate control (**NTC**) and 20 copies/reaction. Example images are shown in **Fig. 5D**. **Fig. 5E** and **5F** shows the software analysed signals from cell phone images under the transilluminator and the glow box, respectively. Classification of the negative from the positive reaction tube images from Scenario 2 taken by all cell phones were excellent (p-value <0.05, nonparametric numerical p-value), except for TecnoB1F (**Fig. 5F,** p-value= 0.079, nonparametric numerical p-value).

3.6. Accuracy validation of assay workflows in contrived RNA spike-in negative human nasal specimens in PBS − Scenarios 1−3

We validated analytical performance of this assay using leftover human nasal specimens that tested negative for SARS-CoV-2. These swabs were previously eluted in 1xPBS buffer. 1x PBS significantly interferes with RT-PCR (**Supplementary Fig. 6A**), where the amplification of spiked SARS-CoV2 RNA at up to 100 copies/reaction was completely inhibited. To ensure successful amplification in less ideal buffer (PBS with nasal matrix), we proceeded with assay validation with samples diluted 4-fold in water, and tested at RNA concentrations of 0, 20, 40, and 100 copies/reaction.

When testing these contrived positive samples at ≥20 copies SARS-CoV-2 RNA using Scenario 1 o 1 (**Fig. 6A**), the N2 assay had 100% sensitivity (41/41, 95% CI: 94.1−100%) and 100% (40/40, 95%

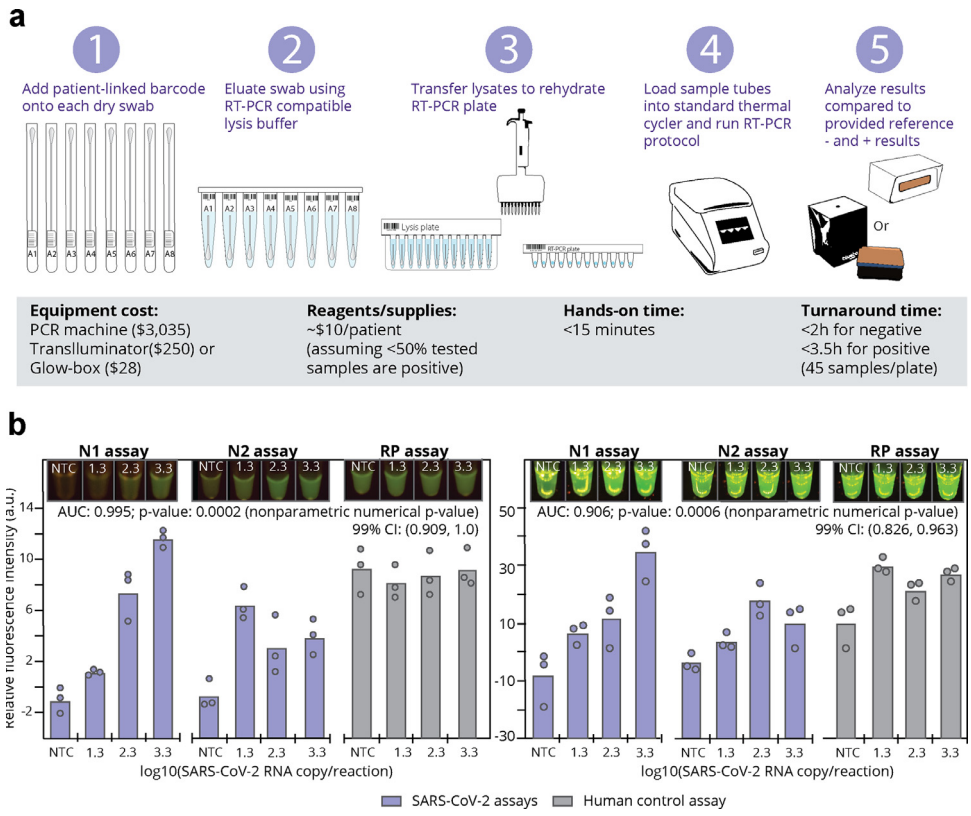

Fig. 3. *Workflow for high-throughput end-point RT-PCR Covid-19 assay for laboratories with access to a 96-well thermal cycler and a fluorescence visualizer* (**A**) Step-wised protocol from step 1−3 are similar to Scenario 1, but the RT-PCR step takes place in a standard thermal cycler. Results are visualised after the completion of RT-PCR step by either a transilluminator *(left)* or battery-powered fluorescence box with an orange filter *(right)*. Equipment costs listed are based on the models we used in this study. (**B**) Analytical sensitivity of the Scenario 2 workflow visualised under a transilluminator. A serial dilution of SARS-CoV-2 RNA spiked in simulated nasal mix at 0 (no template control), 20, 200, or 200 copies/reaction was carried through the Scenario 2 workflow. After the RT-PCR step, images of the tubes visualised under a transilluminator were taken by a cell phone (one replica shown). (**C**) Analytical sensitivity of Scenario 2 workflow visualised under a battery-powered fluorescence box from the same set of RT-PCR products. Each group of data had 3 triplicates. Mean values were reported along with individual data points. P-values and confidence intervals were numerically computed. See details in Section 2.11.

CI: 91.2−100%) specificity. One negative sample was classified as inconclusive, **INC** (i.e. false positive (**FP**) by the N2 assay, true negative by N1 assay, positive by RP assay). We re-ran this sample and did not detect a signal (ID 41) in either of two replicates, suggesting the false positive signal was likely caused by cross-contamination of samples rather than the primer/probe cross-reactivity. All the true positive (**TP**) samples by the N2 assay were successfully detected by the N1 assay. RP assay also successfully amplified all samples with Cq values in our Scenario 1 workflow of 28.2 ± 2.6 (mean ± SD).

For the Scenario 2 workflow, we analysed the end-point fluorescence signal from the images visualised in the transilluminator and captured by the cell phone on the successfully amplified contrived clinical samples, using the software developed for this project (**Fig. 6B**). The end-point results reported analytical sensitivity and specificity of 100% with two (ID 41 from cross-contamination and ID 6) INC results. All samples previously determined as positive in the Scenario 1 workflow were positive, including the N2 assay for the FP sample (ID 41). One additional sample (ID 6) was classified as positive for the N2 assay only. This sample also had high end-point fluorescence in Scenario 1, but was classified as negative by the Bio-Rad software because it was a non-sigmoidal curve.

For the Scenario 3 workflow (**Fig. 6C**), we tested 30 of the 0.25x diluted specimens (30 negative and 30 positives with SARS-CoV-2 RNA spiked in at 20, 40, or 100 copies). N1 and N2 assays had 100% sensitivity (30/30, 95% CI: 88.4−100%) when testing contrived positive samples at ≥20 copies of SARS-CoV-2 RNA and 96.7% (29/30, 95% CI: 82.8−99.9%) specificity when testing contrived negative samples. The one FP sample (ID 6) previously showed non-specific amplification with N2 primers in the Scenario 1 and 2 workflows. **Supplementary Fig. 7** shows images of these reaction tubes.

3.6. Clinical validation of assay workflows in VTM specimens collected from individuals with respiratory symptoms

We validated our modified protocol in 110 VTM specimens. This number of specimens is suitable for high throughput assays; thus, we chose to use the Scenario 1 workflow. **Supplementary Table 6** shows a comparison of Cq values from N1, N2, and RP primers using the standard protocol versus the Scenario 1 workflow. We observed strong correlations (**Fig. 7A-7C**) of Cq values for N1 (R^2 = 0.90, 95% CI: 0.84−0.96, Olkin and Kinn's Approximation) and N2 (R^2 = 0.89, 95% CI: 0.82−0.96) primers using the two protocols. However, we observed less correlation of Cq values (R^2 = 0.29, 95% CI: 0.15−0.42) for RP human control primers. The Scenario 1 workflow detected 35/40 positive specimens, of which one was FN and three were INC by the standard CDC protocol. The five positives misclassified by our modified assay were two FN and three INC, of which one tested INC and four tested positive by the standard protocol. Of 70 negative, our protocol reported 67 TN and 4 indeterminate (**IND**, i.e. samples tested negative by all primers) whereas the standard protocol reported 61 TN and 9 IND (3 were concordant between the two methods). Excluding IND and INC results, clinical sensitivity and sensitivity of Scenario 1 workflow was 94.6% (35/37, CI: 81.8 − 99.3%) and 100% (67/67, 95% CI: 94.6 − 100%). The indeterminate rate of 3.64% (4/110, 95% CI: 1.00 − 9.05%) for the modified protocol is much lower than 8.1% (9/110, 95% CI: 3.8 − 15%) for the standard protocol.

In Section 3.5, we showed that signal from cellphone images obtained from glow box or transilluminator (**Fig. 5B,C**) used in the Scenario 2 and Scenario 3 workflows were highly correlated with the end-point signal from the real-time PCR machine. Building from this finding, we recorded end-point fluorescence signal by the real-time

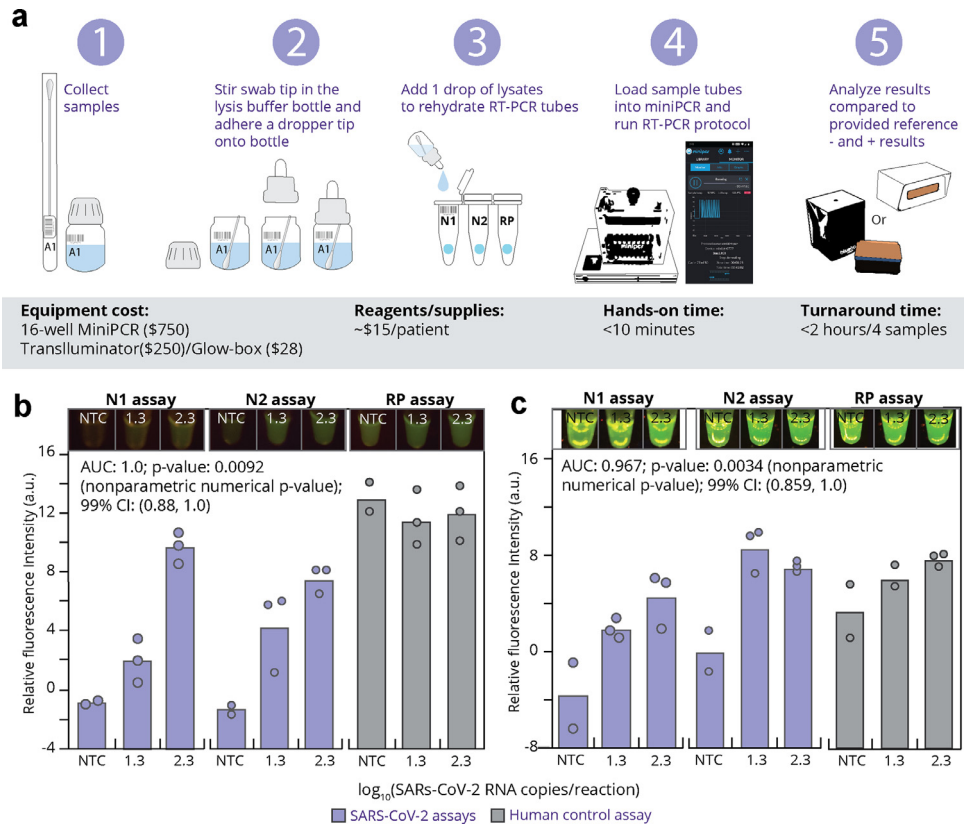

Fig. 4. *Workflow and performance for low throughput for point-of-care settings such as small hospitals or clinics.* (**A**) Step-wise protocol for the Scenario 3 workflow eliminates the need for micropipettes and consistent electricity. Equipment costs listed are based on the models we used in this study. (**B**) Analytical sensitivity of the Scenario 3 workflow visualised under a transilluminator. A serial dilution of SARS-CoV-2 RNA spiked in simulated nasal mix at 0 (no template control), 20, 200, or 2000 copies/reaction was carried through the Scenario 3 workflow. After the RT-PCR step, images of the tubes visualised under a transilluminator were taken by a cell phone (one replica shown). (**C**) Analytical sensitivity of Scenario 3 workflow visualised under a battery-powered fluorescence box from the same set of RT-PCR products. Two replicates for no template control. Three replicates for 20 and 200 copies/reaction. Mean values are plotted with individual data points. Equipment costs listed are based on the models we used in this study. P-values and confidence intervals were numerically computed. See details in Section 2.11.

PCR machine to represent the Scenario 2 workflow. End-point fluorescence results (**Supplementary Fig.8A-8C**) from N1, N2, and RP assays revealed lower sensitivity and specificity than the Scenario 1 workflow. **Supplementary Fig.8D** summarises the qualitative comparison to the standard protocol. Of 40 positive samples 31 were TP, 5 were FN, and 3 were inconclusive (i.e. only detectable by N2). Of 70 negative samples, our assay classified 60 TN, 2 FP; 3 INC, and 5 IND. Overall sensitivity and specificity of the modified protocol using end-point fluorescence was 83.8% (31/37, 95% CI: 68.0 − 93.8%) and 96.8% (60/62, 95% CI: 88.8 − 99.6%), respectively.

4. Discussion

We simplified an existing SARS-CoV-2 RT-PCR through several key innovations. We leveraged lyophilised reagents to bypass the need for manual preparation of master mix and distribution of the master mix into each sample reaction tube at the testing laboratories. We bypassed the RNA extraction step, which is the bottleneck of many laboratories that do not have access to an automatic extraction robot. Finally, we adapted these innovations to equipment appropriate for both high complexity labs and low resource environments. Our simplified methods could benefit laboratories, clinics, and hospitals interested in scaling up and decentralizing SARS-CoV-2 molecular testing, or aid commercial assay developers in designing point-of-care tests where results are useful for clinical care or public health management.

Lyophilization of molecular reactions is essential to enable assay setup by non-trained personnel at the point-of-care; Abbott IDNow®, Cephied Xpert®, and BioFire® FilmArray also take advantage of this technique. We believe the main bottleneck for lyophilization of RT-PCR is the lack of expertise to develop excipient formulations for molecular assays that can maintain high sensitivity and specificity. To eliminate this bottleneck, we have developed and disclosed the excipient formulation compatible with an established US CDC RT-PCR assay. Moreover, lyophilised reagents that have no liquid volume allow for greater sample input and could even further boost sensitivity of this assay.

Our assay bypasses an RNA extraction step by using swab eluate to directly amplify samples. Not only does removing this RNA extraction step reduce turnaround and cost, it also avoids use of toxic reagent, guanidinium thiocyanate (**GuSCN**), a common component of lysis buffer used with all the silica column based kits listed on the CDC protocol and in many point-of-care assays. In the standard CDC protocol, the RNA extraction step is crucial to remove any RT-PCR inhibitors, namely fetal bovine serum and antibiotics present in VTM. In this study, we suggest transport of dry swabs that are introduced into mild lysis buffer to enable extraction-free, direct amplification. Use of dry swabs can eliminate the need for VTM, which has seen supply shortage due to high demand of SARS-CoV-2 testing. Detection of SARS-CoV-2 directly from dry swabs has been used in some EUA tests including the Abbott IDNow® [21]. We used a relatively high concentration of RNAse inhibitors that can deactivate endogenous RNAses during the mild heating step at 55 °C for reverse transcription. Moderate heat in conjunction with mild detergents (i.e. Triton X-100, NP-20, and Tween-20) have been shown to lyse virus and human cells [22-24]. Here, we show that ≤1% of these detergents do not negatively impact our RT-PCR, and 0.5% triton-X100 and 55 °C during reverse transcription were sufficient to open the viral

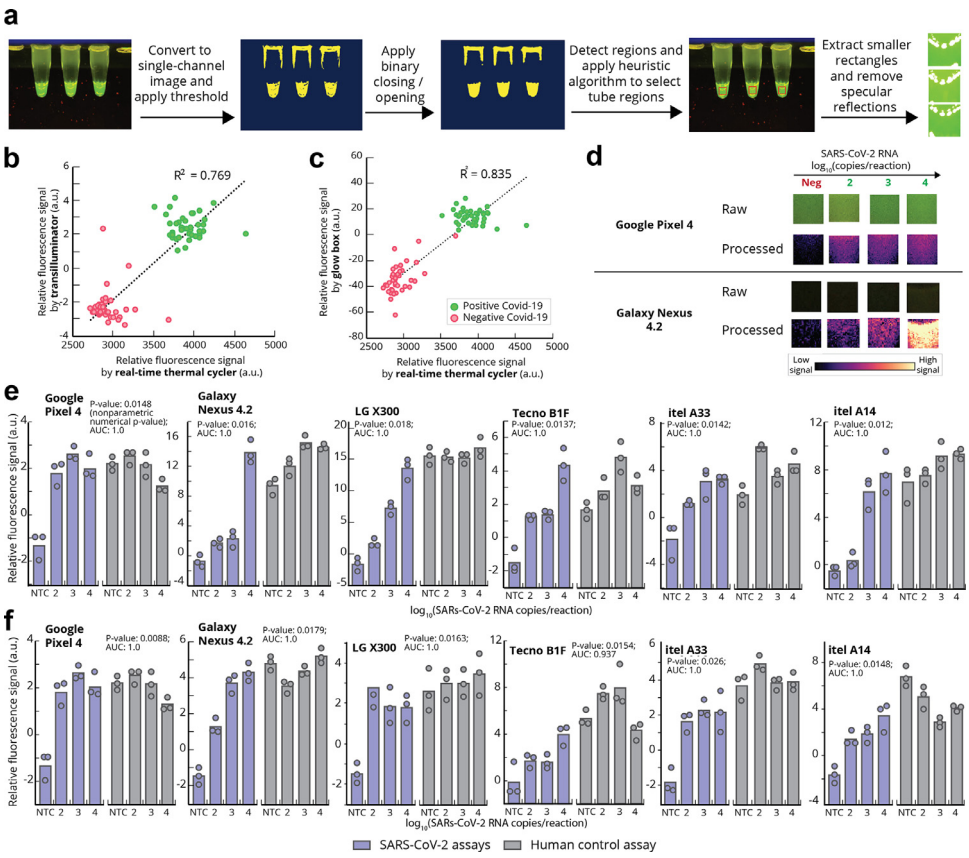

Fig. 5. Software analysis of fluorescence tube images (**A**) Image processing algorithm workflow for an example image from the glow box at 2000 copies/reaction. Details of the algorithm are in the method section. (**B**) Correlation plot of end-point fluorescence intensity read by the real-time thermal cycler and the signal from the transilluminator and (**C**) from the glow box. (**D**) Comparison of processed image examples (support-vector machine projected pixels) and their original images under the transilluminator. (**E**) Comparison of software analysis of images by different models of cell phones under transilluminator and (**F**) under the glow box. These images were taken from RT-PCR products that underwent the Scenario 2 workflow. Samples were SARs-CoV-2 RNA spiked in the simulated nasal swab lysate at 0 (NTC: no template control), 20, 200, or 2000 copies/reaction in the N2 and RP assay (3 technical replicates with mean). Each circle represents individual data points. All processed ROI of images from each cell phone model are available in **Supplementary Fig. 4**.

envelope of the control virus and release RNA, with detection of 25 SARS-CoV-2 RNA copies/reaction. The volume of swab elution buffer required will depend on the absorbency of swabs [25], geometry of the buffer containers, and the level of inhibitors that may be present in the patient specimens. The first two factors can be determined by the assay developers, but the interference levels may vary across individual clinical samples. For the mid-turbinate swab used in our study, we determined an elution volume of 300 μL-1000 μL based on the lysis buffer container used in our workflow. We successfully detected 20 copies of RNA/reaction in the presence of simulated nasal matrix, which corresponds to 300−1000 RNA copies/swab sample. This level of sensitivity may already be sufficient to detect SARS-CoV-2 in the early days after the onset of symptoms (peaked at 10^4 RNA copies/nasopharyngeal swab and 10^7 RNA copies/throat swab [26]).

Direct amplification of contrived nasal swab PBS eluates by this test showed 100% sensitivity at ≥20 copies/reaction and 96.7%−100% specificity using all three workflows. Overall sensitivity and specificity of this test are similar to other RT-PCR tests that received US FDA EUA [27] when processing similar types of contrived samples. In this study, we were limited by the swab elution buffer used in these left-over specimens (i.e. PBS). We found that salt (137 mM NaCl) in the PBS in combination with clinical nasal matrices caused RT-PCR inhibition, and dilution factors of 0.25x or 0.5x were needed to rescue amplification of the human RP control. Whilst further dilution of PBS is not ideal, the results served as promising strategies for direct amplification. Both N1 and N2 assays in 0.25x PBS sensitively detected down to 20 copies/reaction.

For direct comparison with the CDC protocol using clinical nasal specimens stored in VTM, we used a 0.25x dilution factor to directly amplify VTM samples in lyophilised RT-PCR. This 0.25x concentration of VTM is higher than the 0.07x− 0.1x VTM concentrations used in other studies for direct amplification [28, 29], suggesting that our RT-PCR may tolerate inhibitory substances better than other RT-PCR assays. The Scenario 1 workflow compared well to the CDC standard protocol with 94.6% sensitivity and 100% specificity. Of the four positive samples not detected by the modified protocol, three had low target concentrations (<5 copies/reaction): two were INC (Cq: 37.7, 37.3; not detected, 40.8 by N1 and N2 standard protocol, respectively) and one was FN (Cq: 41.9, 38.3). One FN had a high copy (>200 copies/reaction; Cq: 20.7, 21.9) but was not detectable, likely due to high concentration of PCR inhibitors in this sample. Surprisingly, IND occurred much less in our protocol than in the standard protocol (3.6% vs 8.2%), while INC results were comparable (2.7% vs 3.6%). Technically RNA extraction removed any inhibitors from the nasal samples, and we expected a higher amplification yield. However, the Scenario 1 workflow showed that only 1/110 samples were likely to have benefitted by this step.

In addition to developing the assay chemistry for lyophilization and direct amplification, we developed three workflows aimed at three different equipment sets and designed to cover most common laboratory setups that could run the assay. The Scenario 1 workflow is most analogous to what is currently done in medium to high complexity laboratories with access to real-time thermal cyclers. A 96-well plate can screen up to 45 samples (if 6 wells are used for negative and positive controls). This screening approach would reduce the overall assay cost compared to the CDC protocol. The Scenario 2 workflow drops the equipment cost around 10 fold by removing the need for a real-time thermal cycler, making it less cost-prohibitive to

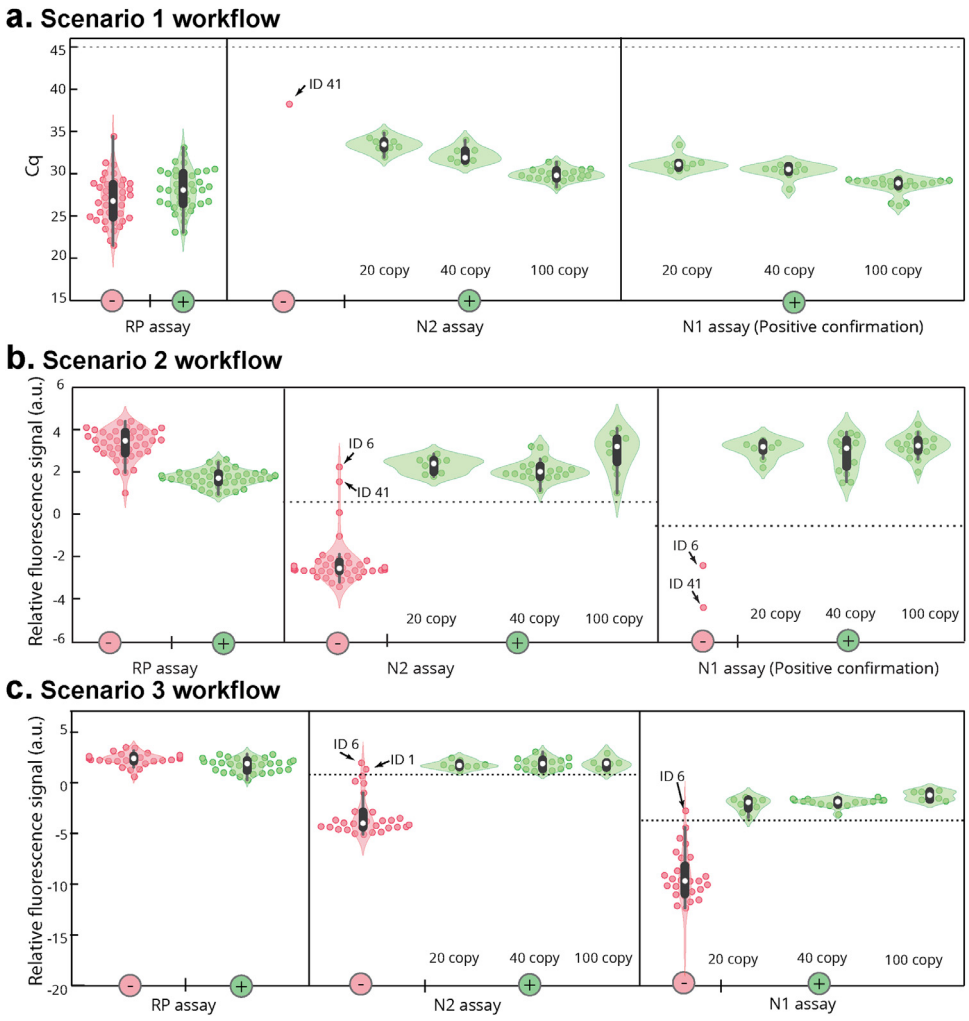

Fig. 6. *Validation of contrived clinical specimens in 0.25x PBS.* Each of 41 human nasal swab eluates were used to generate a pair of negative and positive samples. Positive samples were spiked with purified SARS-CoV-2 RNA at 20, 40, and 100 copies/reaction. Both positives and negatives were run on both N2 and N1 (SARS-CoV-2 detection) and RP (human control) RT-PCR assays. (**A**) Scenario 1 workflow was used to process this panel of specimens. Cq (quantification thresholds) of each sample from N2, N1 and RP assays were plotted. (**B**) Images of the RT-PCR products generated in (**A**) were captured under the transilluminator to mimic the outcome of the Scenario 2 workflow. Dotted lines show the positive thresholds for N2 and N1 primer assays. (**C**) Due to a low-throughput capacity of the Scenario 3 workflow, we tested 30 samples. Images of the reaction tubes were captured under the glow box. Dotted line is the positive threshold for N1 and N2 assays. The mean of each group is presented as the white circle with interquartile range box as well as range. The density distribution is also shown.

perform a high-throughput assay, in exchange for an additional step of end-point fluorescence signal analysis. End-point detection of RT-PCR may lead to false positive results. For analysis of contrived specimens in human matrix using end-point fluorescence results in the Scenario 3 workflow, 1/30 samples had false positive due to non-specific amplification in a sample with high amount of mucus, which cannot be differentiated from the true positive, whereas manual inspections of real-time RT-qPCR curves can help rule out non-specific amplification because true positives have a characteristic sigmoidal amplification curve. We also observed similar non-sigmoidal signals in 3/70 negatives when analyzing the clinical nasal specimens in VTM.

The Scenario 3 workflow was designed for the lowest resource environment, and may be useful as a point-of-care, low-throughput RT-PCR testing. The use of a battery-powered, low-cost thermal cycler enables reliable Covid-19 testing in low-resource settings where power outage is common. We observed that the battery-powered thermal cycler performed 10-minutes slower than the traditional 96-well thermal cycler, but this additional time delay may not significantly impact the clinical management of patient care. The battery-powered, low-cost glow box also improves resilience to power outages, but with the tradeoff of poorer signal to the unaided eye compared to the transilluminator. However, with the help of software image processing, negative samples can be differentiated from 20 copies/reaction, providing similar results to those from transilluminator images. To further explore the limitations of our fluorescence classification software and the robustness of the approach across different phone models, we tested the software using images captured by six additional cell phone models commonly used in low-resource settings. The images had varied quality for capturing the fluorescence signal. Some phone models also have incorporated features in the camera that may affect the image analysis. In addition to the phone models, it is also noteworthy to mention that the room light conditions could add artifacts to the pictures taken. In this study, we kept the image-taking process consistent, but further testing using different phone models under various conditions should be performed to ensure robustness of data collection and analysis.

Besides the thermal cycler and fluorescence reader, micropipettes are impractical for point-of-care settings. Instead, our Scenario 3 workflow uses an inexpensive bottle with a dropper adapter to dispense lysates to the dry reagents and requires no specialised training. This bottle has a larger dead volume than the swab elution tubes used in Scenario 1 and 2 workflows, causing us to adjust the swab elution volume to 1000 μL instead of 300 μL. The dead volume could

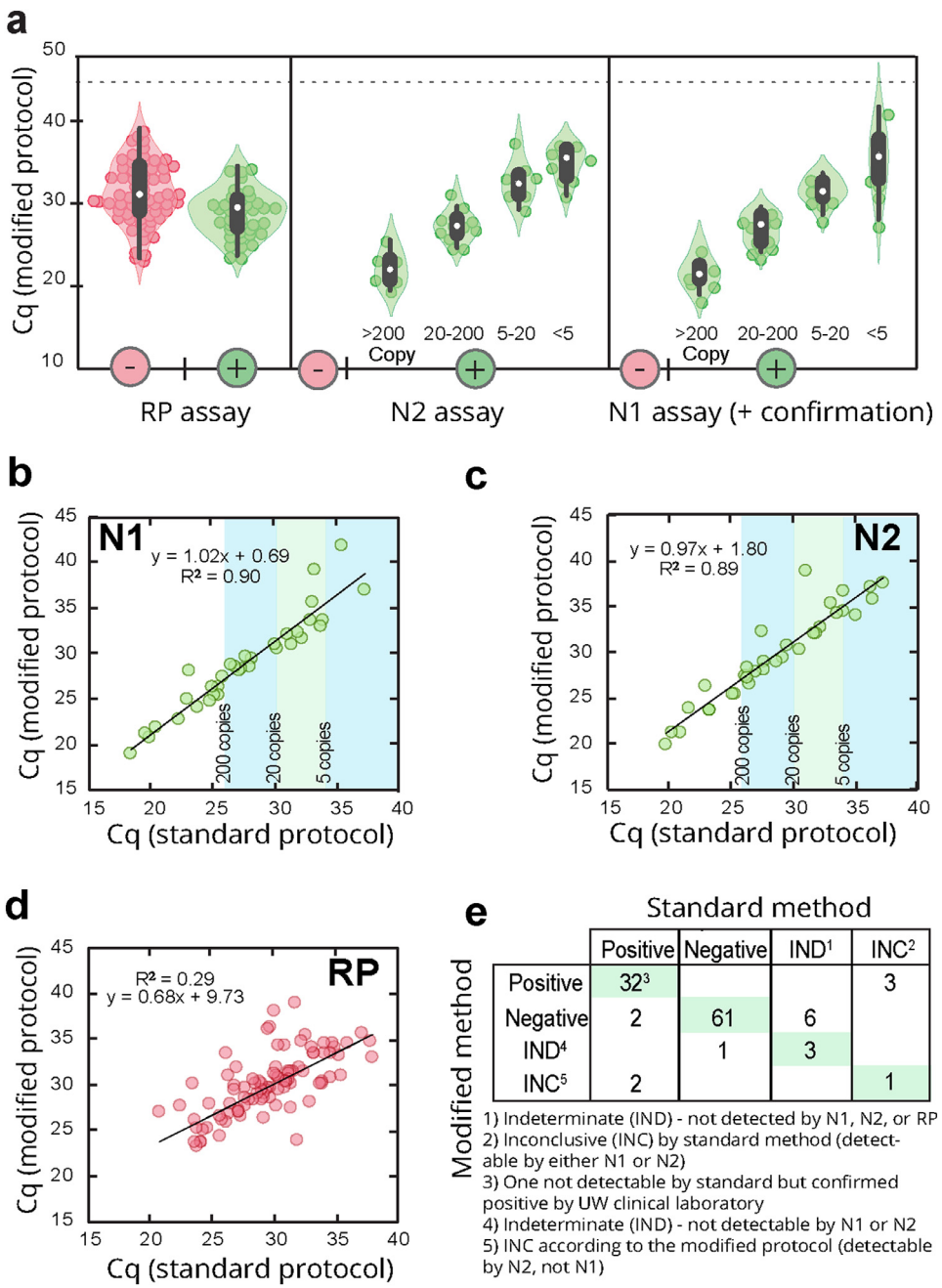

Modified method \ Standard method	Positive	Negative	IND[1]	INC[2]
Positive	32[3]			3
Negative	2	61	6	
IND[4]		1	3	
INC[5]	2			1

Fig. 7. *Validation of our modified protocol (Scenario 1 workflow) on clinical VTM specimens.* (**A**) C_q values of N1, N2, and RP modified protocol. Dotted lines show the positive thresholds for N2 and N1 primer assays. The mean of each group is presented as the white circle with interquartile range box as well as range. The density distribution is also shown. C_q values of the (**B**) N1, (**C**) N2 assay, and (**D**) RP assay was compared to those obtained by the CDC standard protocol. (**E**) Qualitative comparison of positive, negative, indeterminate (**IND**), inconclusive (**INC**) results from our modified protocol vs standard protocol.

be reduced with a narrower bottle. Whilst there are still changes that can be made to optimize this workflow, its simplicity makes it a promising platform for RT-PCR at the point-of-care. The relatively economical list of required materials makes it a low cost and highly scalable alternative to other point-of-care products. A single Abbott IDNow® machine costs as much as ~20 battery-powered thermal cyclers that can test 80 clinical samples in two hours, compared to 8 samples for Abbott IDNOW® (one specimen/15 min). Moreover, we have gathered the information for commercial equipment that could be used for the three workflows presented (**Supplementary Tables 2**–**5**), but without access we did not validate our assays on all of the equipment. However, we showed that the assay chemistry is sufficiently robust across a battery powered thermal cycler, a standard thermal cycler, and a real-time thermal cycler. This is a promising indicator that this assay should be suitable for use in other commercially available thermal cyclers.

At the time that we wrote this manuscript, we were working to develop interactive software to guide technicians in performing these three laboratory workflows. A collaboration is set to begin demonstration of these workflows in comparison to the standard CDC protocols at several sites in the USA. Previously, we have used the software guidance at sites in Kenya and the US to operate a more complicated workflow successfully. We used Aquarium, which is a web-based human-in-the-loop laboratory automation application that integrates inventory tracking, data collection, experimental protocols, and workflow management [30]. We are transforming our SARS-CoV-2

RNA detection lab procedures into guided Aquarium protocols to gain the advantages of laboratory automation, data collection, and protocol distribution. We envision that our high-performance SARS-CoV-2 diagnostic workflows encoded as Aquarium protocols will facilitate the rapid deployment of low-cost and efficient Covid-19 testing sites.

Contributors

NP conceived the idea of the assay workflows. NP, QW, and AKO designed, conducted, and analysed RT-qPCR experiments. QW captured cell phone images of fluorescent tubes. PSR wrote the Python code for automating image fluorescence extraction from tube images. IB tested nasal swab specimens using CDC EUA assay in the CLIA-certified SCRI lab and provided left-over eluate for clinical validation study. JHK arranged the cell phone loan from Michael Maruchek from Audere that we used to study software. JHK and SWAS researched and summarised the information from the EUA-approved kits, and developed the list of open-sourced, commercial equipment. AM and JV discussed the Aquarium software design for assay workflows. PDH and LMS designed and characterised a panel of clinical samples for assay evaluation. LMF and BRL oversaw the study design. All authors provided feedback on data analysis and interpretation, contributed in writing this manuscript and approved the final version of this manuscript.

Data sharing statement

All data involved in this study are available in the main text and supplementary information.

Declaration of Interests

Authors have no conflict of interest to declare.

Acknowledgments

We thank other Lutz lab members: Enos Kline, Ian Hull, Mike Roller, Robert Atkinson, and Daniel Leon; researchers from the Seattle Flu Study: Dr. Jay Shendure and Dr. Jase Gehring for technical support and helpful discussion. We thank Dr. Lucia Vojtech, Dr. Gaurav Gulati, and Dr. James Lai for the quantitation of the RNA standards using digital droplet PCR. We thank Audere for lending different cell phones to capture the images of the tubes in this study. We thank Dr. Eric Klavins and his lab members, Dr. Devin Strickland and Dr. Benjamin J Keller, for the collaboration and stimulating discussion on Aquarium software development. We thank the University of Washington Statistics Consulting Services for their advice on estimation of confidence interval of non-parametric numerically p-value. We thank Elizabeth Mounce for her help identifying and purchasing the materials used in this study.

Supplementary materials

Supplementary material associated with this article can be found, in the online version, at doi:10.1016/j.ebiom.2021.103236.

References

[1] Rhoads D.D., Cherian S.S., Roman K., Stempak L.M., Schmotzer C.L., Sadri N. Comparison of Abbott ID Now, Diasorin Simplexa, and CDC FDA EUA methods for the detection of SARS-CoV-2 from nasopharyngeal and nasal swabs from individuals diagnosed with COVID-19. J Clin Microbiol. 2020;58(8):e00760-20.
[2] U.S. Food & Drug Administration. Coronavirus (COVID-19) Update: FDA Authorizes First Antigen Test to Help in the Rapid Detection of the Virus that Causes COVID-19 in Patients. 2020.
[3] Procop G.W., Brock J.E., Reineks E.Z., Shrestha N.K., Demkowicz R., Cook E., et al. A comparison of five SARS-CoV-2 molecular assays with clinical correlations. Am J Clin Pathol. 2020;155(1):69-78.
[4] Basu A. Estimating the infection fatality rate among symptomatic COVID-19 cases in the United States. Health Aff. 2020;39(7) 101377hlthaff202000455.
[5] Bai Y, Yao L, Wei T, Tian F, Jin D-Y, Chen L, et al. Presumed asymptomatic carrier transmission of COVID-19. JAMA 2020;323(14):1406–7.
[6] Hu Z, Song C, Xu C, Jin G, Chen Y, Xu X, et al. Clinical characteristics of 24 asymptomatic infections with COVID-19 screened among close contacts in Nanjing, China. Sci China Life Sci. 2020;63(5):706–11.
[7] Lee Y.N. 7 charts show how the coronavirus pandemic has hit the global economy. 2020. https://www.cnbc.com/2020/04/24/coronavirus-pandemics-impact-on-the-global-economy-in-7-charts.html.
[8] Siddarth D., Weyl E.G. Why We Must Test Millions a Day Edmond J. Safra Center for Ethics 2020 [6:[Available from: https://ethics.harvard.edu/files/center-for-ethics/files/white_paper_6_testing_millions_final.pdf?m=1586798243.
[9] U.S. Food & Drug Administration. EUA Authorized Serology Test Performance 2020; 1331-1338. [updated 2020/7/5. Available from: https://www.fda.gov/medical-devices/emergency-situations-medical-devices/eua-authorized-serology-test-performance.
[10] Nagura-Ikeda M, Imai K, Tabata S, Miyoshi K, Murahara N, Mizuno T, et al. Clinical evaluation of self-collected saliva by quantitative reverse transcription-PCR (RT-qPCR), direct RT-qPCR, reverse transcription-loop-mediated isothermal amplification, and a rapid antigen test to diagnose COVID-19. J Clin Microbiol 2020;58(9) e01438−20.
[11] FIND. SARS-CoV-2 diagnostic pipeline 2020 [Available from: https://www.finddx.org/covid-19/pipeline/?section=molecular-assays.
[12] U.S. Centers for Disease Control and Prevention. 2019-Novel Coronavirus (2019-nCoV) Real-time rRT-PCR panel primers and probes. Atlanta, GA: U.S.: Department of Health and Human Services; 2020 May 29, 2020.
[13] U.S. Centers for Disease Control and Prevention. CDC 2019-Novel Coronavirus (2019-nCoV) real-time RT-PCR diagnostic panel for emergency use only. 2020 December 1st, 2020. Contract No.: CDC-006-000019. https://www.fda.gov/media/134922/download.
[14] Panpradist N, Beck IA, Vrana J, Higa N, McIntyre D, Ruth PS, et al. OLA-Simple: a software-guided HIV-1 drug resistance test for low-resource laboratories. EBioMedicine 2019;50:34–44.
[15] Panpradist N, Beck IA, Ruth PS, Avila-Rios S, Garcia-Morales C, Soto-Nava M, et al. Near point-of-care, point-mutation test to detect drug resistance in HIV-1: a validation study in a Mexican cohort. AIDS 2020.
[16] U.S. Centers for Disease Control and Prevention. CDC 2019-Novel Coronavirus (2019-nCoV) Real-Time RT-PCR Diagnostic Panel (Instructions for Use). 2020 December 12th, 2020. Contract No.: CDC-006-00019.
[17] Nuttada Panpradist, Bhushan J., Toley, Xiaohong Zhang, Samantha Byrnes, Joshua R., Buser, Janet A., Englund, Barry R. Lutz. "Swab Sample Transfer for Point-Of-Care Diagnostics: Characterization of Swab Types and Manual Agitation Methods". September 2, 2014. doi: 10.1371/journal.pone.0105786.
[18] Rogers J.H., Link A.C., McCulloch D., Brandstetter E., Newman K.L., Jackson M.L., et al. Characteristics of COVID-19 in homeless shelters: a community-based surveillance study. Ann Intern Med. 2020; M20-3799, Epub Ahead of Print.
[19] Olsson C, Jansson H, Swenson J. The role of Trehalose for the stabilization of proteins. J Phys Chem B 2016;120(20):4723–31.
[20] Cepheid. 510(k) Substantial Equivalence Determination Decision U.S. Food & Drug Adminstration. Report No.: K180218. https://www.accessdata.fda.gov/cdrh_docs/reviews/K180218.pdf.
[21] Abbott. ID NOW COVID-19 Quick Reference Instructions 2020 [Available from: https://www.alere.com/en/home/product-details/id-now-covid-19.html.
[22] Li L, He J-A, Wang W, Xia Y, Song L, Chen Z-H, et al. Development of a direct reverse-transcription quantitative PCR (dirRT-qPCR) assay for clinical Zika diagnosis. Int J Infect Dis 2019;85:167–74.
[23] Srivatsan S., Han P.D., van Raay K., Wolf C.R., McCulloch D.J., Kim A.E., et al. Preliminary support for a "dry swab, extraction free" protocol for SARS-CoV-2 testing via RT-qPCR. https://www.biorxiv.org/content/10.1101/2020.04.22.056283v1.
[24] Smyrlaki I., Ekman M., Vondracek M., Papanicoloau N., Lentini A., Aarum J., et al. Massive and rapid COVID-19 testing is feasible by extraction-free SARS-CoV-2 RT-qPCR. medRxiv. 2020.
[25] Panpradist N, Beck IA, Chung MH, Kiarie JN, Frenkel LM, Lutz BR. Simplified paper format for detecting HIV drug resistance in clinical specimens by oligonucleotide ligation. PLoS One 2016;11(1):e0145962.
[26] Woelfel R, Corman VM, Guggemos W, Seilmaier M, Zange S, Mueller MA, et al. Clinical presentation and virological assessment of hospitalized cases of coronavirus disease 2019 in a travel-associated transmission cluster. Nature 2020;58:465−469.
[27] International I. Smart Detect™ SARS-CoV-2 rRT-PCR Kit 2020 2020 [Available from: https://inbios.com/smart-detecttm-sars-cov-2-rrt-pcr-kit/.
[28] Bruce E.A., Huang M.L., Perchetti G.A., Tighe S., Laaguiby P., Hoffman J.J., et al. Direct RT-qPCR detection of SARS-CoV-2 RNA from patient nasopharyngeal swabs without an RNA extraction step. bioRxiv. 2020.
[29] Smyrlaki I, Ekman M, Lentini A, Rufino de Sousa N, Papanicolaou N, Vondracek M, et al. Massive and rapid COVID-19 testing is feasible by extraction-free SARS-CoV-2 RT-PCR. Nat Commun 2020;11(1):4812.
[30] Keller B., Vrana J., Miller A., Newman G., Klavins E. Aquarium: the Laboratory Operating System (Version v2.5.0). Zenodo 105281/zenodo2535715. 2019.